Modelling of hot tearing: two-phase models, coalescence and mesoscale granular models

J.-M. Drezet, M. Sistaninia and M. Rappaz

Computational Materials Laboratory, LSMX
Ecole Polytechnique Fédérale de Lausanne
CH–1015 Lausanne, Switzerland

Table of content

Hot tearing in solidification processes

Semi-continuous casting for extrusion billet and rolling sheet ingots

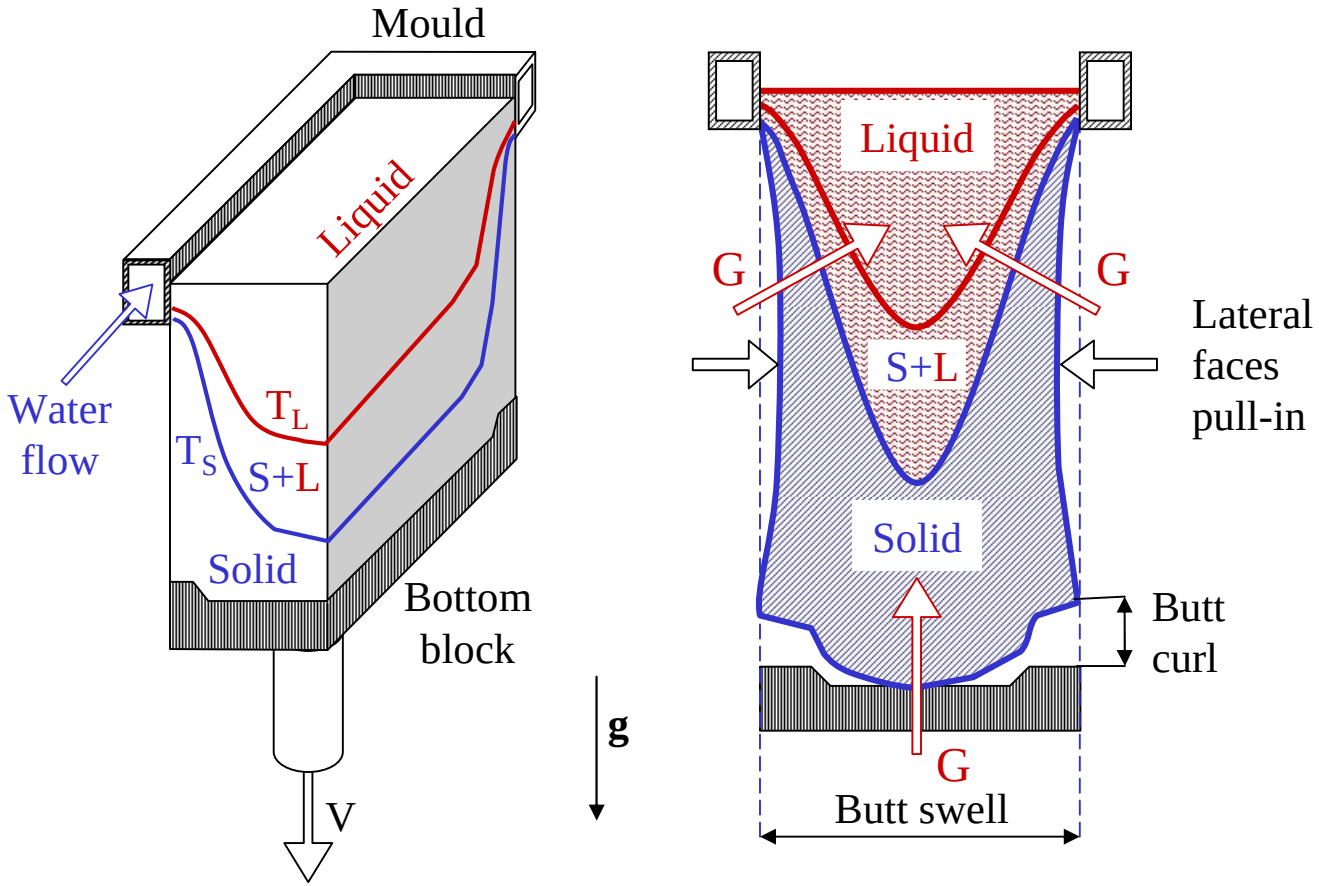

Hot tearing in solidification processes

In extrusion billet and rolling sheet ingots, hot tearing limits the productivity for some particular alloys.

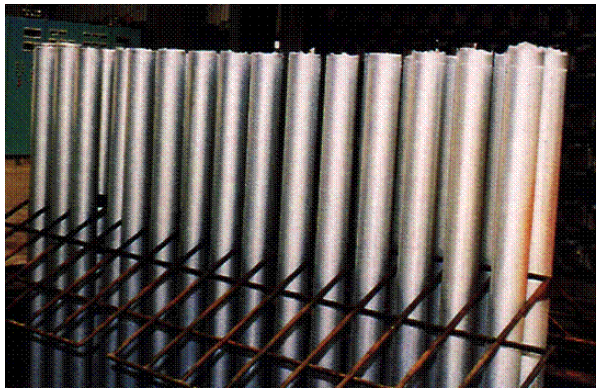

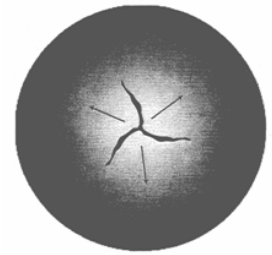

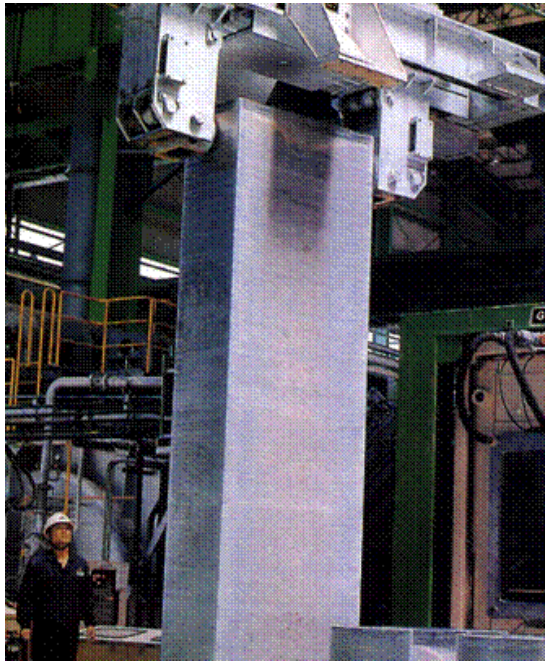

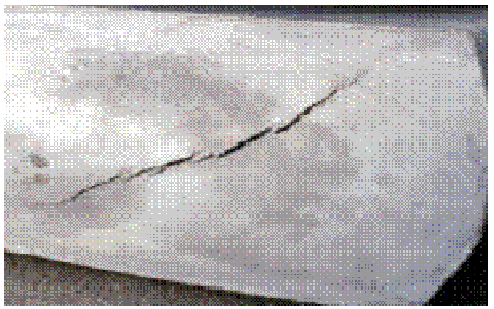

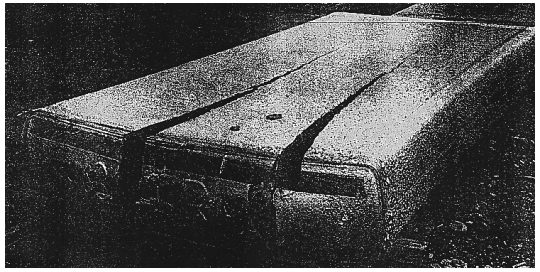

Laser beam welding (LBW):

to replaces riveted sections with welded integral structures

major drawbacks: hot cracking and porosity, especially in transients (run-in and run-out) for lighter Al-Li alloys

use of filler wire

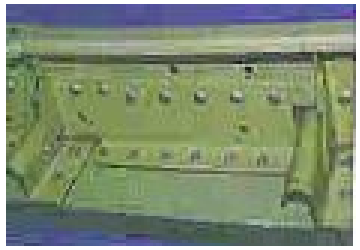

• Phénomène intergranulaire

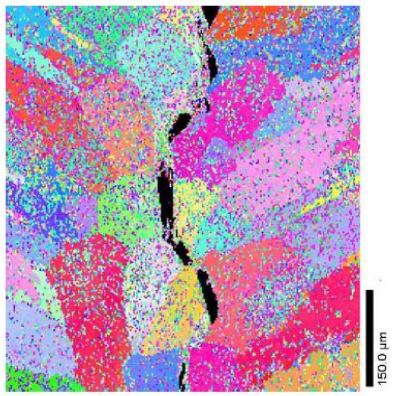

LB welding of AA6056 + AA4047 (Al-Si): final Si content varies between 1.5 and 4 % (D. Fabrègue)

Hot tearing tests:

TIG welding of AA6061 aluminium alloy

application of a tensile deformation along the fusion line

(Aurélie Niel, C. Bordreuil and G. Fras, LMGC, Univ. Montpellier)

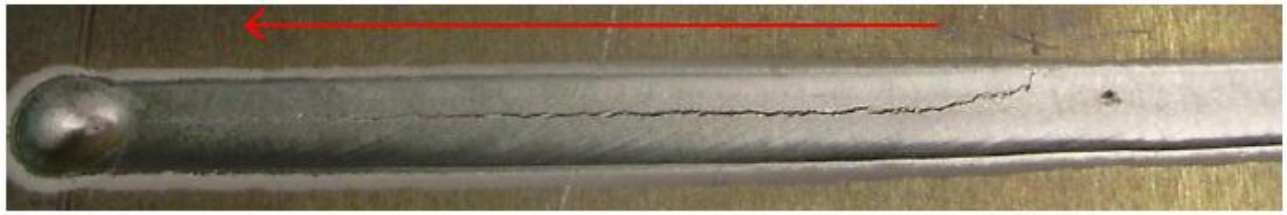

EB welding of a CuCrZr alloy:

D. Ayrault (CEA), J. Wisniewski, PhD 2009, UBS

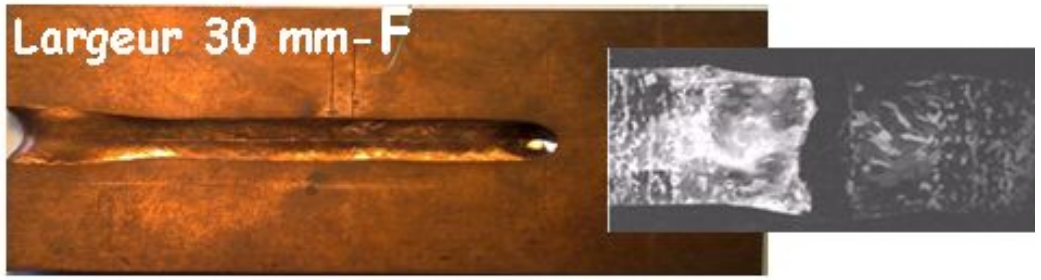

EB welding of a CuCrZr alloy:

J. Wisniewski, PhD 2009, UBS and CEA

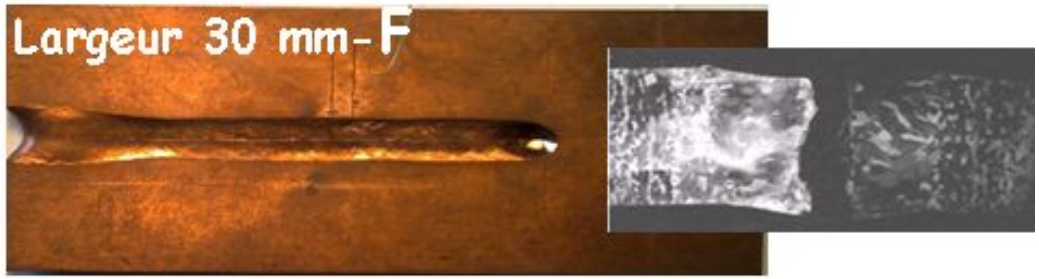

Essais JWRI fissurant
(largeur 30 mm)

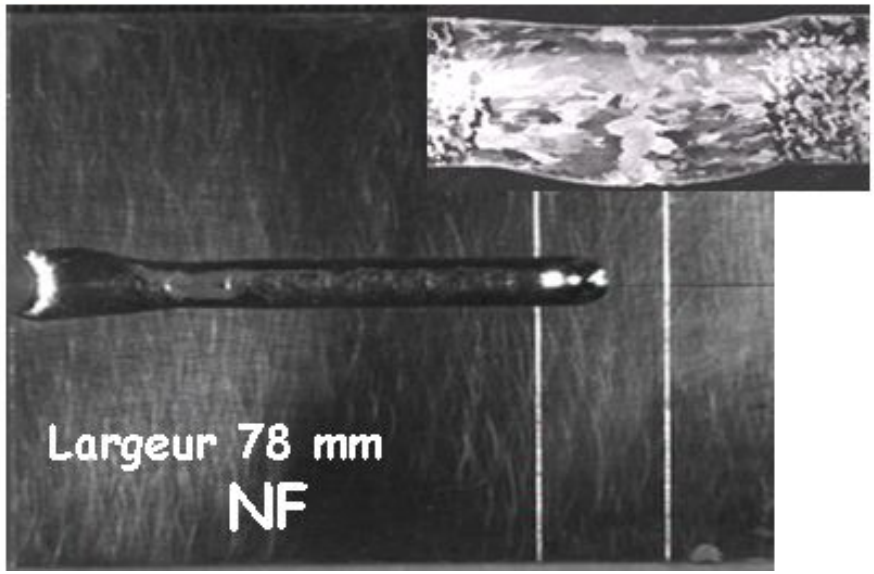

et non fissurant
(largeur 78 mm)

Laser welding of aluminium alloys using two laser beams:

W. Kurz et al., patent EP 01810986.8

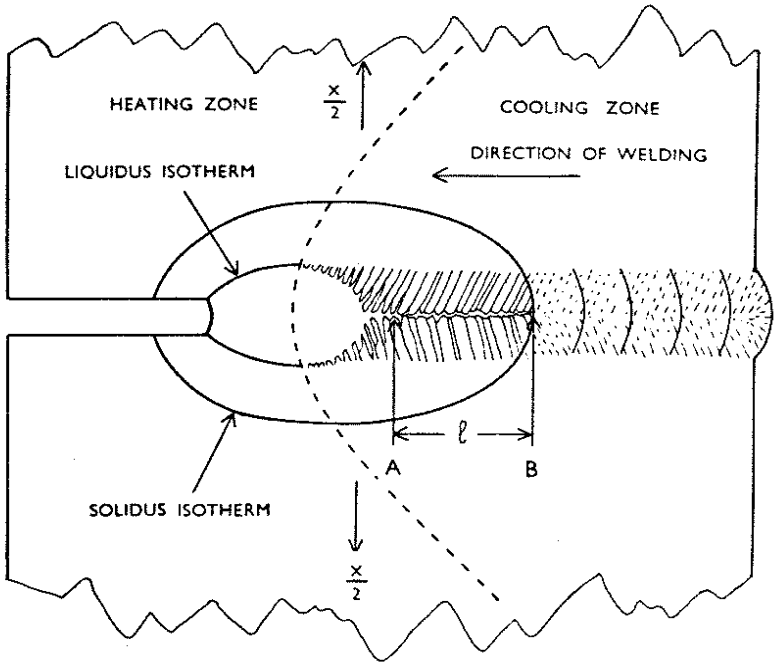

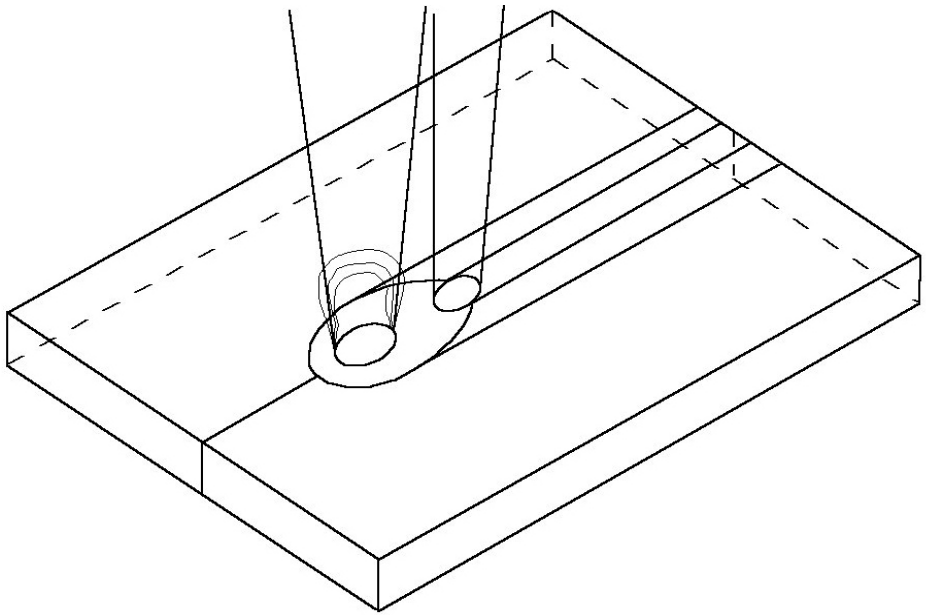

Without any filler materials.

Control of thermal loading and thus of microstructure formation by promoting the CET

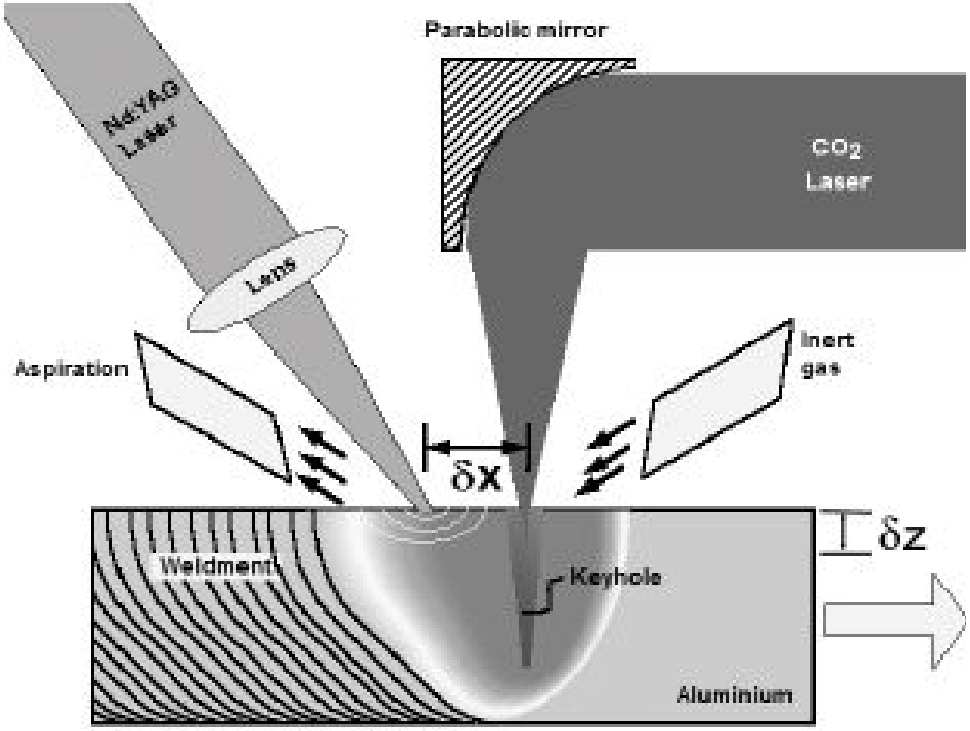

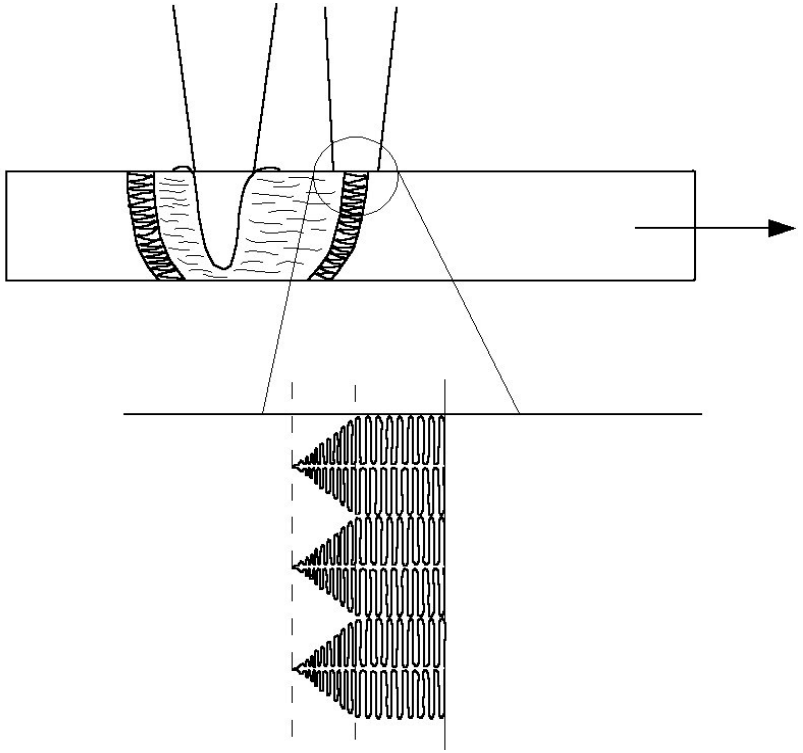

Microstructure and hot tearing

X-ray imaging of dendritic growth in binary alloys

(RH Mathiesen and L. Arnberg, Phy. Rev. Letters, vol. 83, no. 24, 1999.)

Columnar growth in Sn-Pb 10wt. Pct.

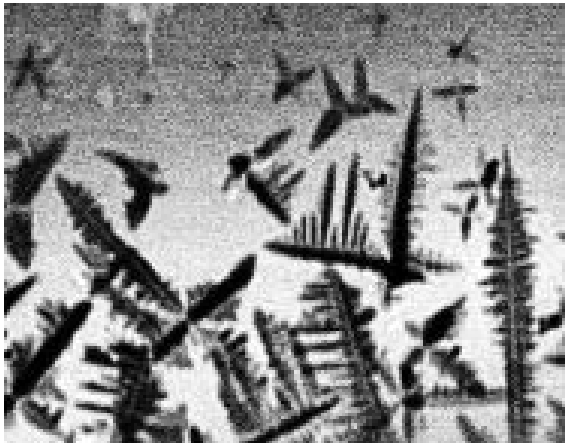

Equiaxed growth in Sn-Pb 52 wt. pct

CET: Columnar to equiaxed transition

Film on transparent alloy (Succinonitril-acetone)

Increased weldability is observed with the use of the double source: continuous 1.4 kW CO2 laser + pulsed Nd-YAG laser at the rear

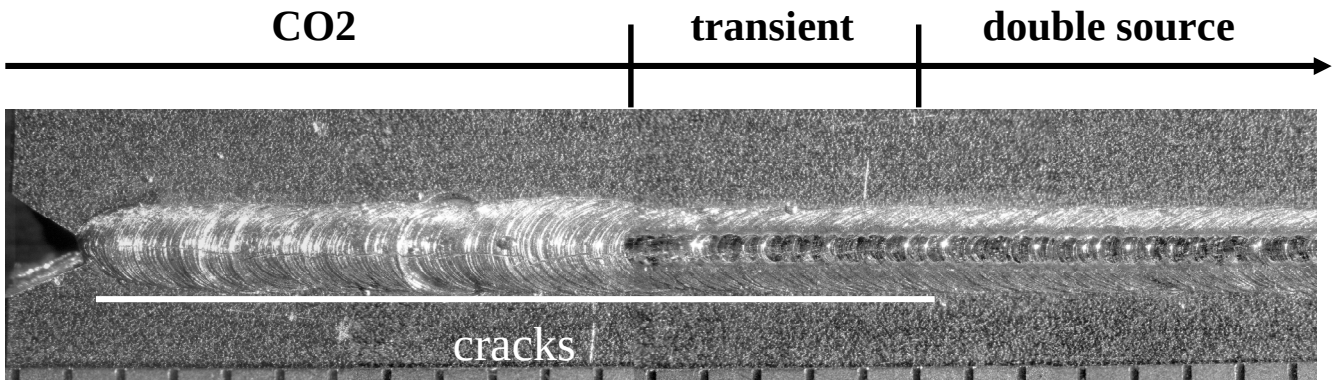

CO2 zone

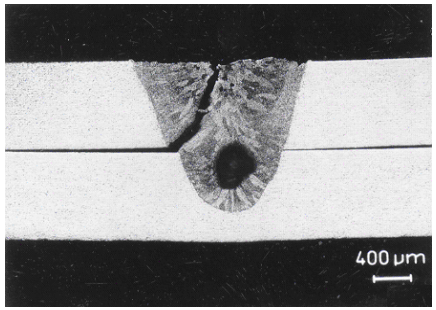

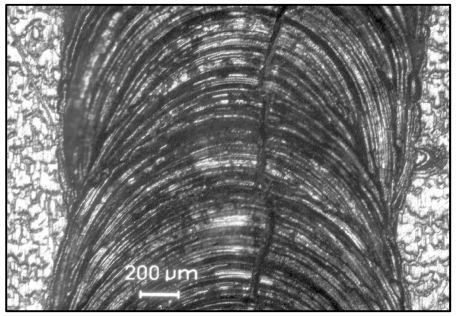

Double source zone

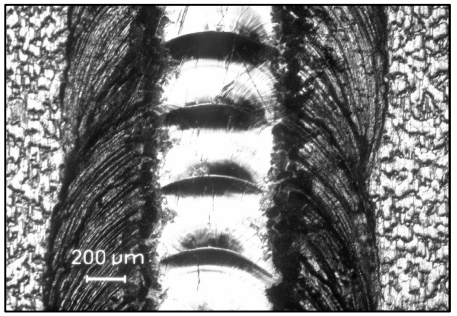

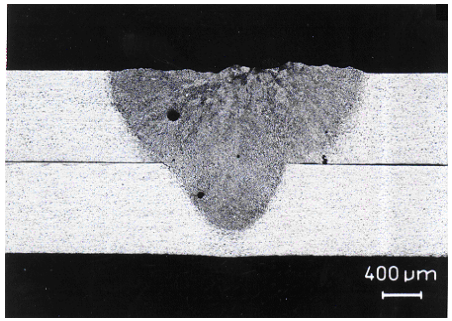

Increased weldability: hot tears disappear

Vb = 60 mm/s, P_{CO2} = 1400 W, He 4 l/min, dx = -2.5 mm

Foc_{YAG} = -1 mm, E = 3 J, f = 150 Hz, P_{YAG} = 450 W, tp = 1 ms

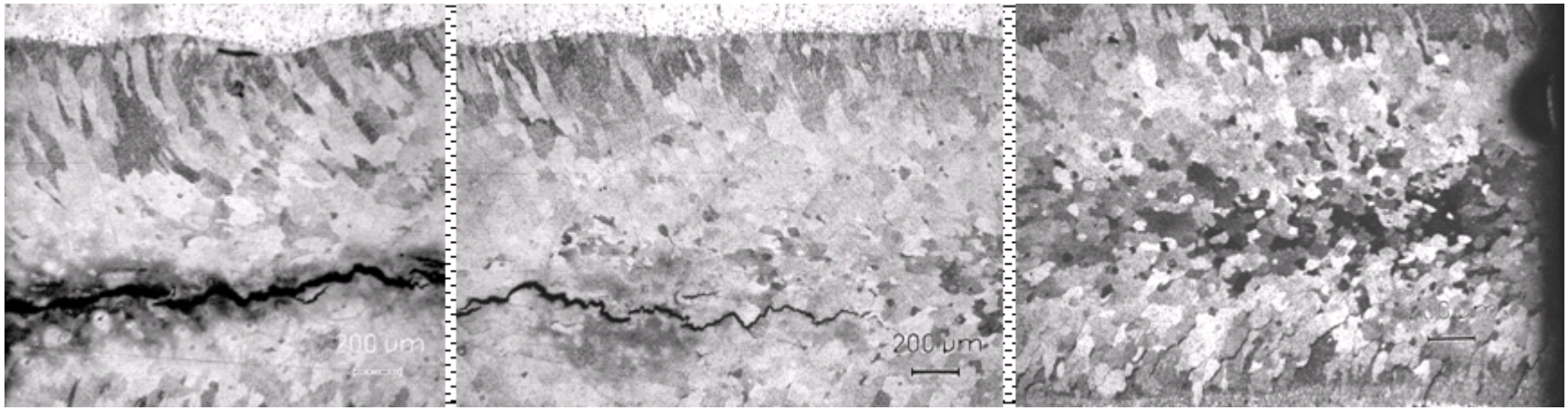

200 µm

CO_2 Transient CO_2 + YAG

Two-phase approaches

Physical quantities are averaged over the solid and liquid phases (density and mass flow rate)

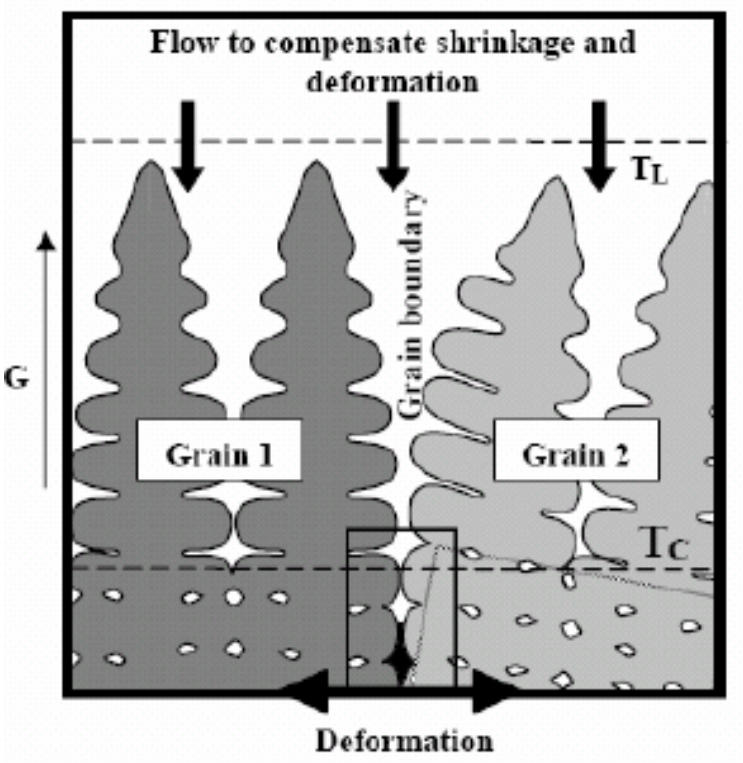

$$\langle \rho \rangle = g_s \rho_s + g_l \rho_l$$

$$\langle \rho \vec{v} \rangle = g_s \rho_s \vec{v}_s + g_l \rho_l \vec{v}_l$$

Two-phase approach: RDG criterion

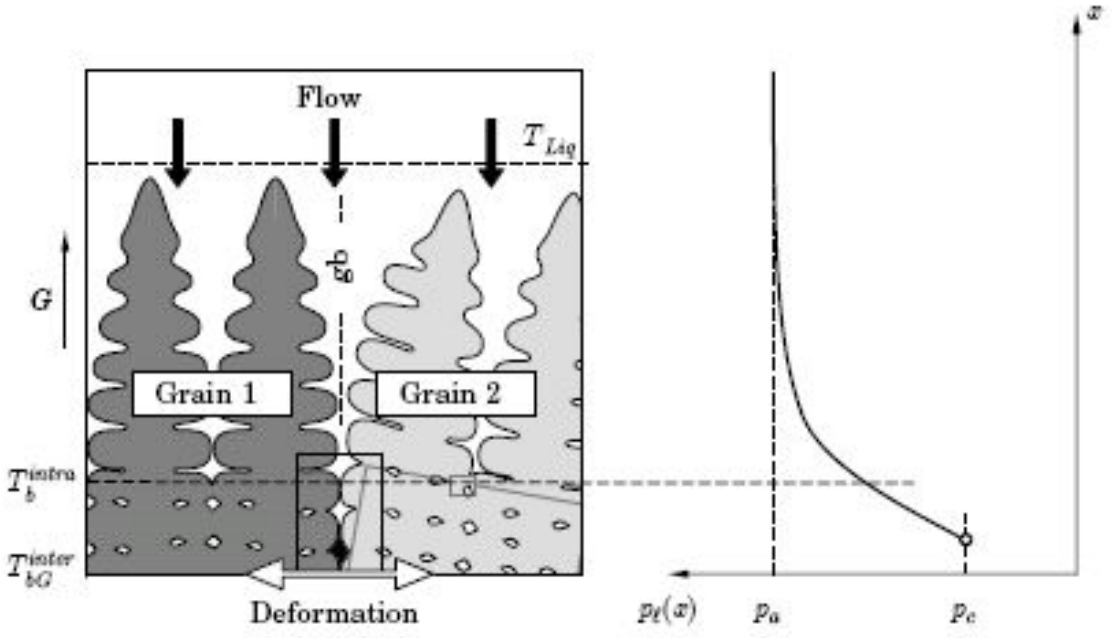

The RDG approach makes a balance between:

- the solidification shrinkage
- the deformation of the mush
- and the possible liquid feeding.

Two-phase approach: mass balance

solidification shrinkage

deformation of the mush

liquid feeding

$$\rho \frac{\partial g_s}{\partial t} + (1+\beta) g_s (\dot{\varepsilon}_{yy} + \dot{\varepsilon}_{zz}) = div\left(\frac{K}{\mu} (gradP_l - \rho_l g) \right)$$

In steady state: determination of the pressure drop within the liquid films

$$\Delta p_{\max} = (1+\beta)\mu \int_0^L \frac{E}{K} dx + v_T \beta \mu \int_0^L \frac{g_l}{K} dx \leq \Delta p_{cavitation}$$

$$E(x) = \int g_s (\dot{\varepsilon}_{yy} + \dot{\varepsilon}_{zz}) dx$$

Two-phase approach: U ductility curve

RDG: the strain rate undergone by the mush is limited.

Critical slope of the thermomechanical path during welding (CST)

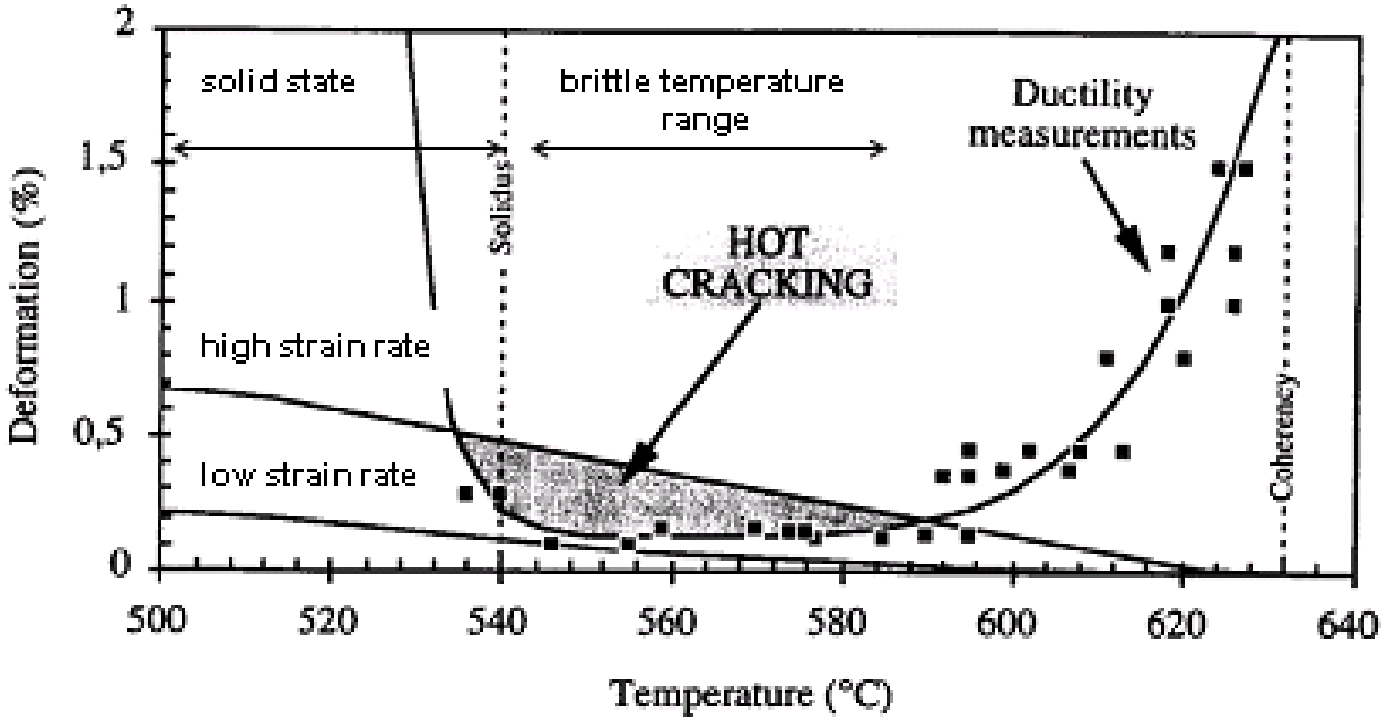

$$\frac{\partial \varepsilon}{\partial T} = \frac{\partial \varepsilon}{\partial t} * \frac{\partial t}{\partial T} = \frac{\dot{\varepsilon}}{\dot{T}}$$

Hot cracking susceptibility: HCS

The RDG allows us to rank the alloys according to their HCS using the A and B integrals (linked to their feeding ability):

$$\Delta p_{sh} + \Delta p_{mec} = \frac{180\mu}{G\lambda_2^2}\left[v_T \beta A + \frac{(1+\beta)B\dot{\varepsilon}}{G} \right]$$

$$A = \int_{T_{cg}}^{T_{liq}} \frac{f_s^2 dT}{(1-f_s)^2} \quad \text{and} \quad B = \int_{T_{cg}}^{T_{liq}} \frac{f_s^2 \int_{T_{cg}}^{T} f_s dT}{(1-f_s)^3} dT$$

Difficulty: determination of Tcg

NB: A and B diverges when Tcg approaches Tsol.

Influence of a filler wire on HCS

AA4047 (AlSi12) together with AA2098 (Al-3.66%Cu-0.33%Mg-0.99%Li)
Solidification paths computed by ProPhase (Pechiney, CRV) under Scheil's conditions

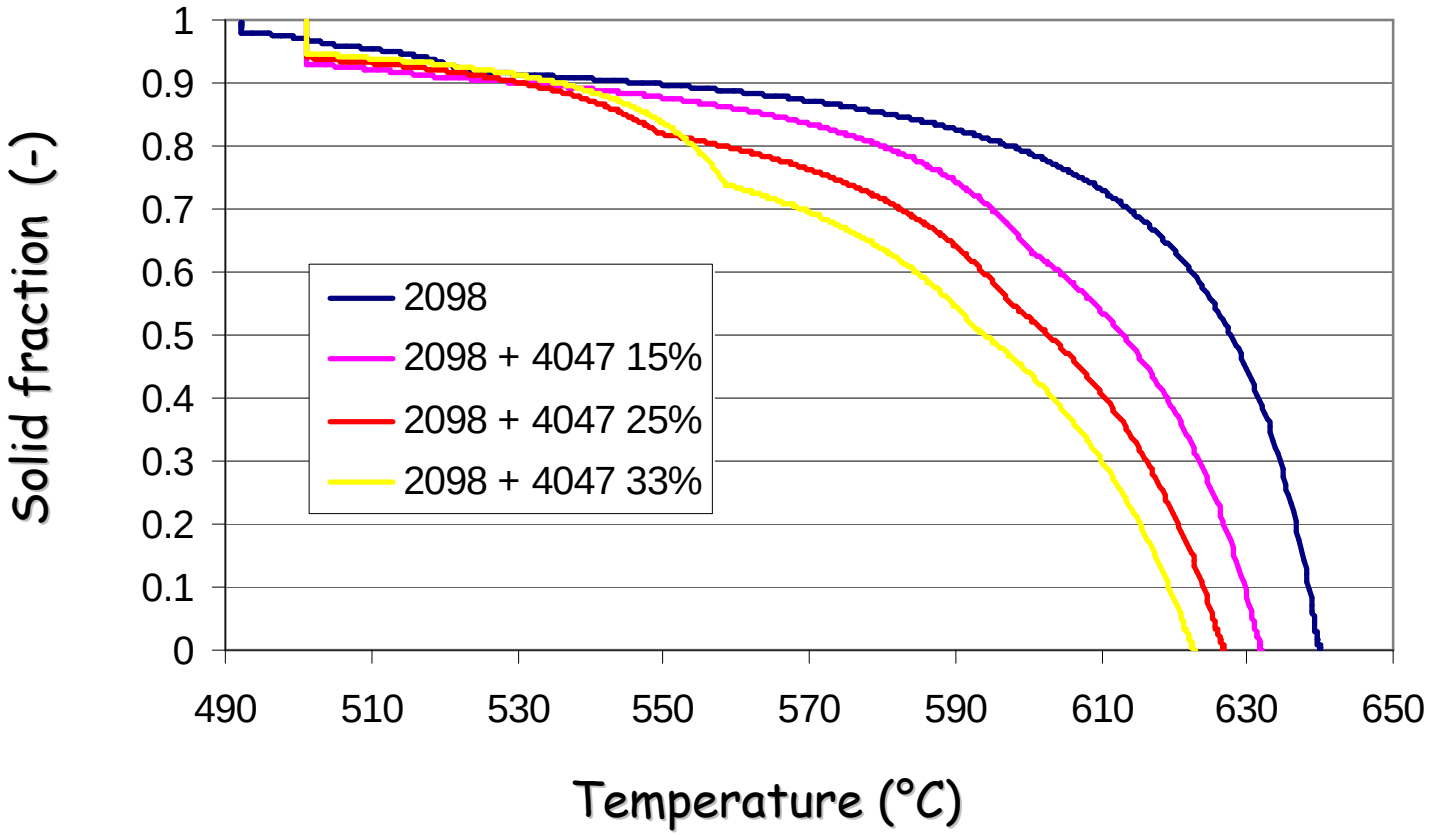

Influence of the filler material (AlSi12):

almost 6 times less prone to HT

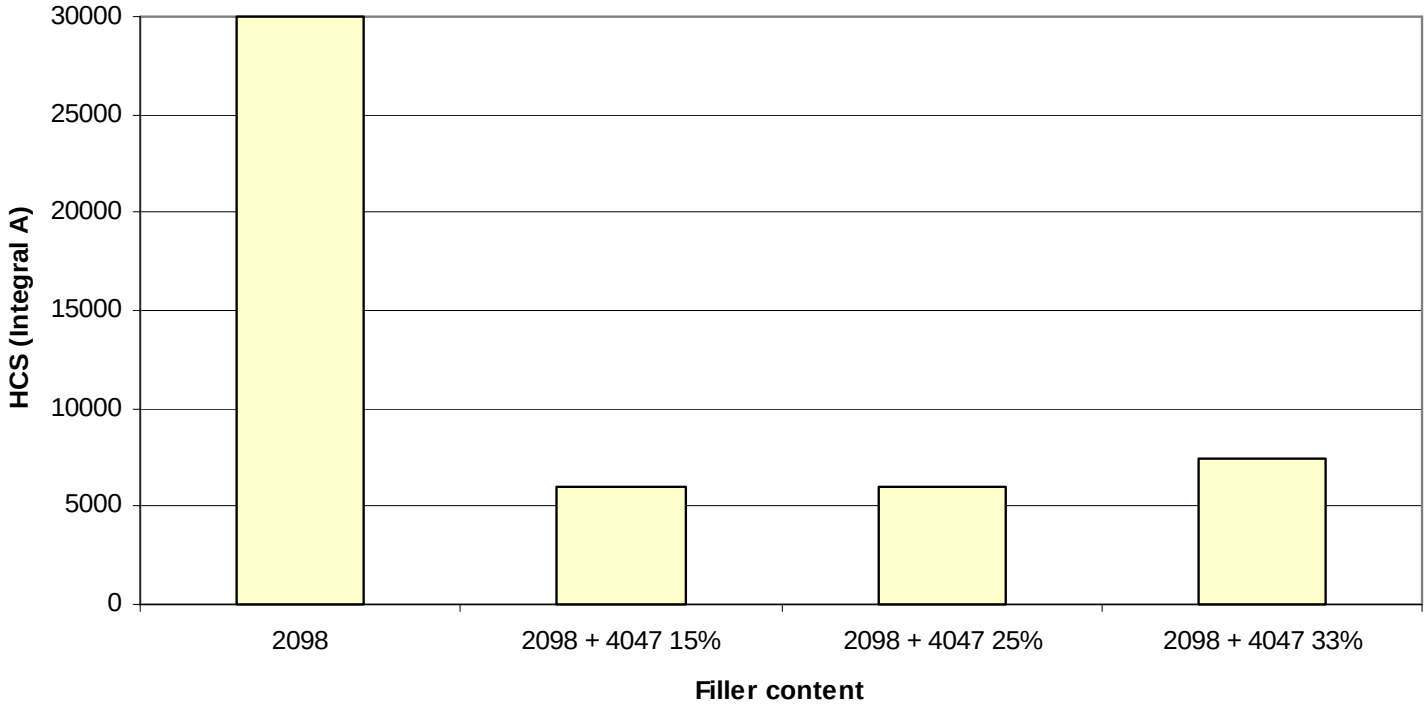

Thermal hot cracking criterion

The pressure drop within the liquid films must remain lower than the cavitation pressure:

$$\Delta p_{max} = \Delta p_{sh} + \Delta p_{mec} - \rho g h \leq \Delta p_{cav}$$

$$\dot{\varepsilon}_p \leq \dot{\varepsilon}_p^{max}(G, V_T, A, B, \Delta p_{cav}, \lambda_2, ...)$$

$$HCS = \frac{1}{\dot{\varepsilon}_p^{max}}$$

Thermo-mechanical approach

The rheology of the solid+liquid mixture must be known to determine the pressure drop within the liquid films.

As compressibility of the medium has to be considered, complex constitutive models have been set up for mushy alloys.

As a first step, the strain rate tensor within the BTR can be used as a hot tearing indicator:

$$\Delta p_{sh} + \Delta p_{mec} = \frac{180\mu}{G\lambda_2^2}\left[v_T \beta A + \frac{(1+\beta)B(\dot{\varepsilon}_{xx} + \dot{\varepsilon}_{yy})}{G} \right]$$

Coalescence of dendrites and grains

One of the main problems in hot tearing is COALESCENCE or BRIDGING of the primary phase.

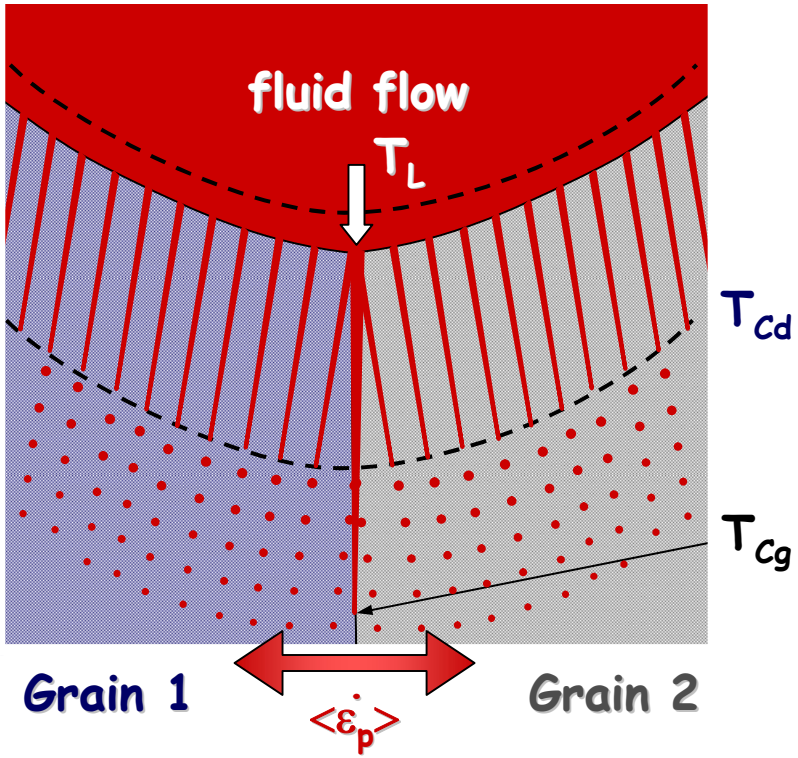

In columnar structures, coalescence within the grains occurs at $T_{Cd} > T_{Cg}$ at grain boundaries.

This leads to a strain localisation...

... and to a localisation of feeding.

An undercooling is needed to "weld" the repulsive grains: $\Delta T_b = \frac{1}{\Delta s_f} \frac{\gamma_{gb} - 2\gamma_{sl}}{\delta}$

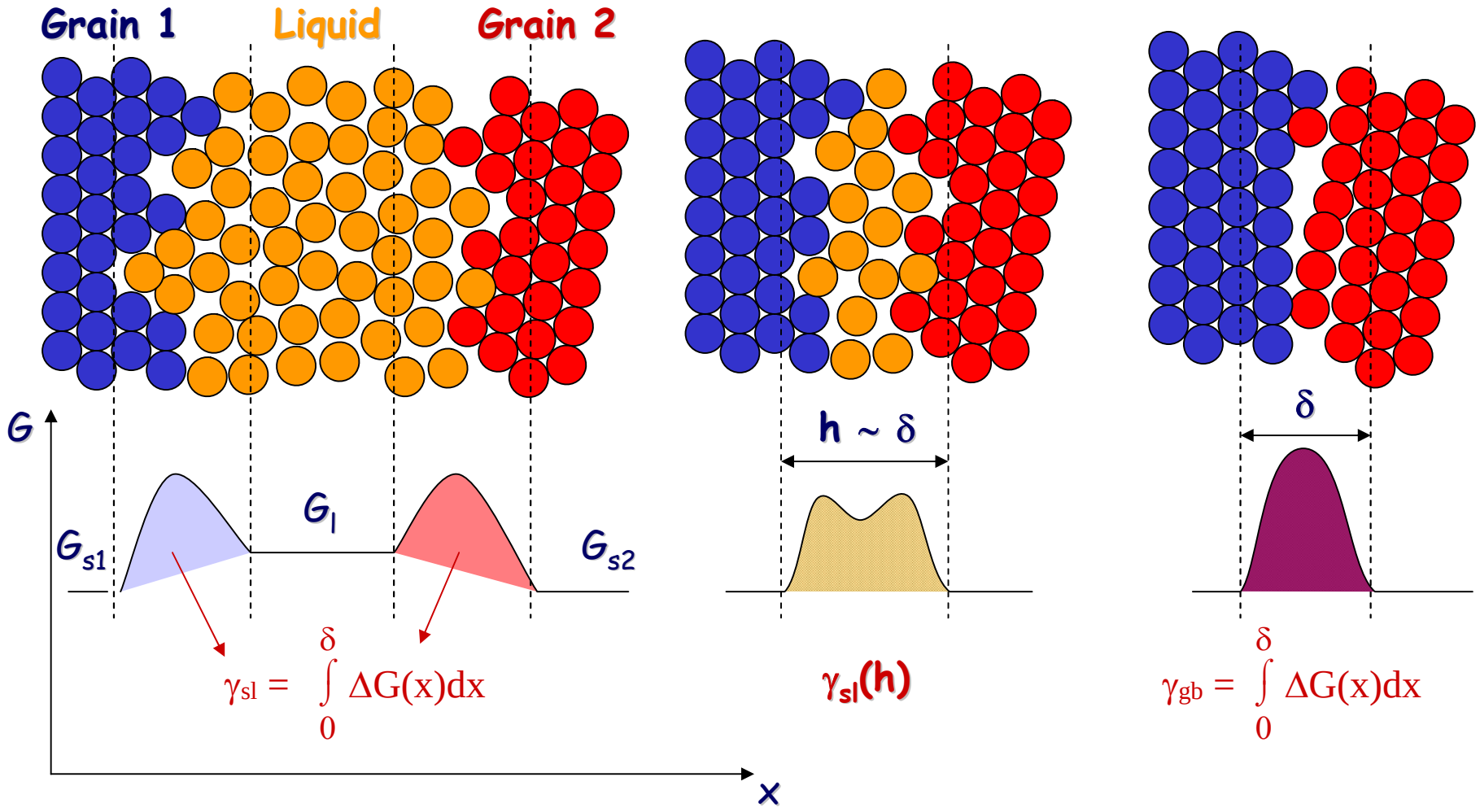

Importance of the coalescence of grains with regard to hot tearing

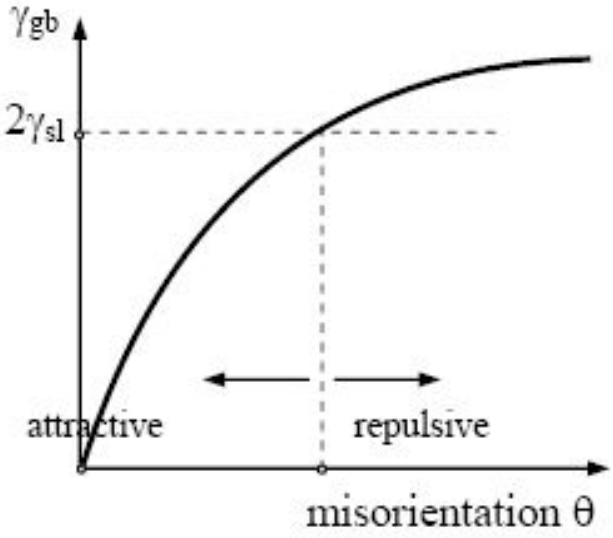

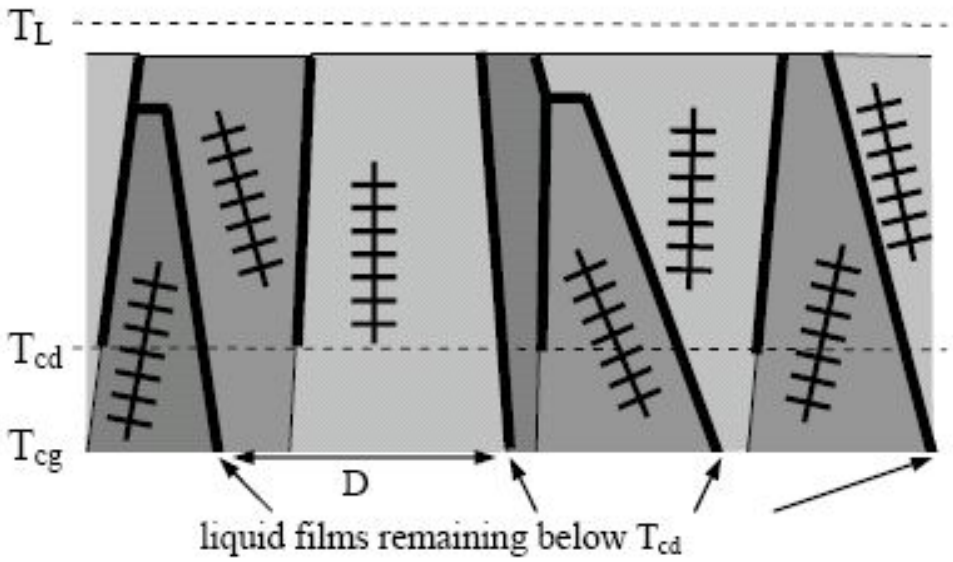

The critical misorientation at which $\gamma_{gb} = 2\gamma_{sl}$ defines the transition between attractive and repulsive grain boundaries.

Centre line weld crack

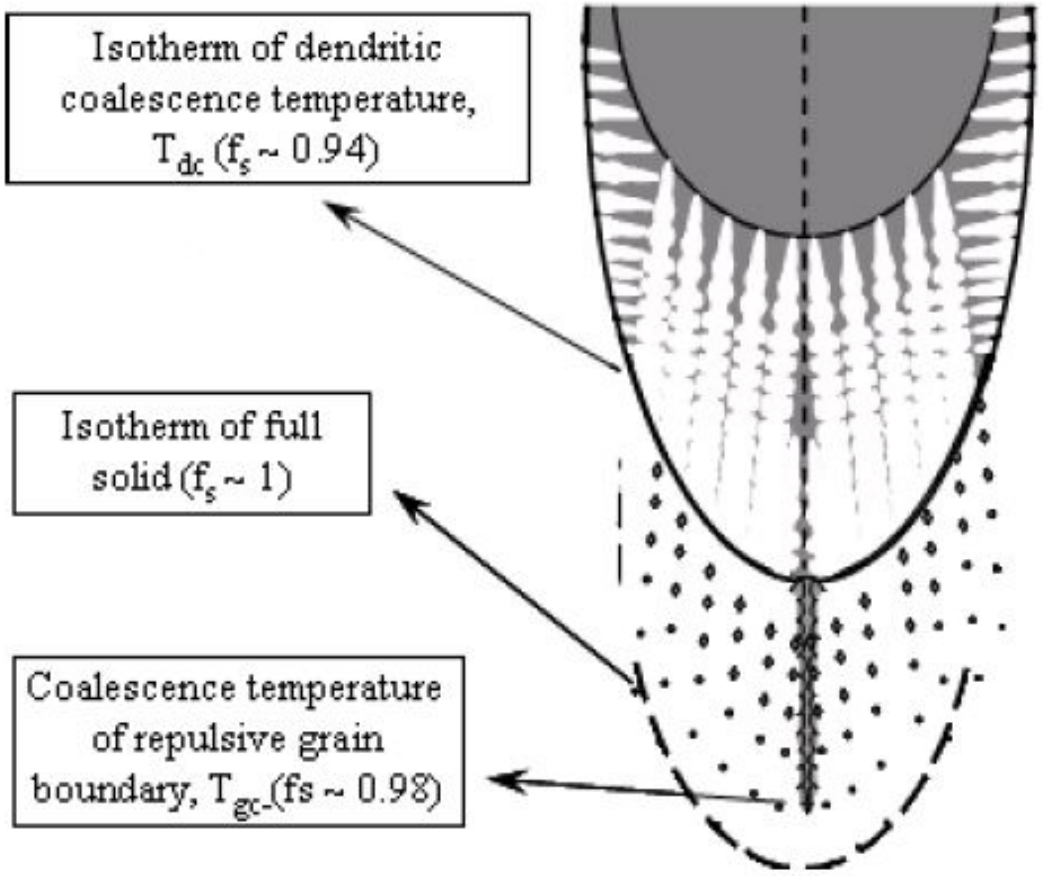

For attractive grain boundaries (no misorientation), the coalescence temperature is located at the same location as in a single crystal.

For repulsive grain boundaries, coalescence takes place at a much lower temperature. This leads to the survival of a liquid film deep into the mushy zone.

Strain localisation on that liquid film might give birth to solidification cracking.

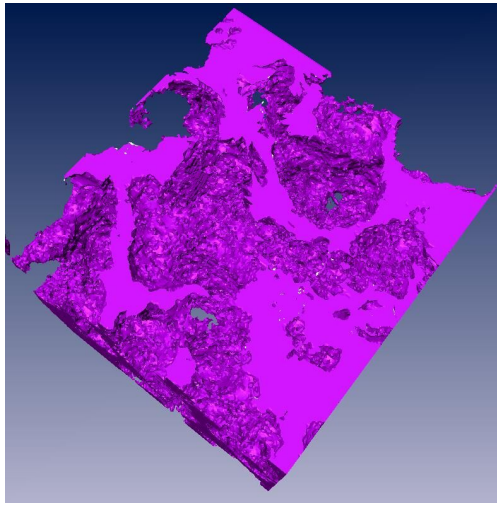

635°C (59%)

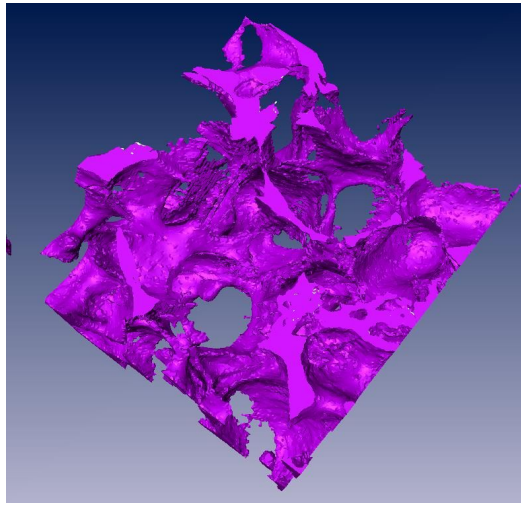

604°C (85%)

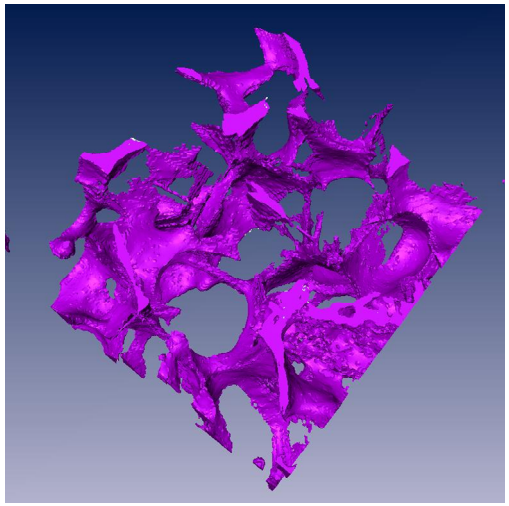

582°C (92%)

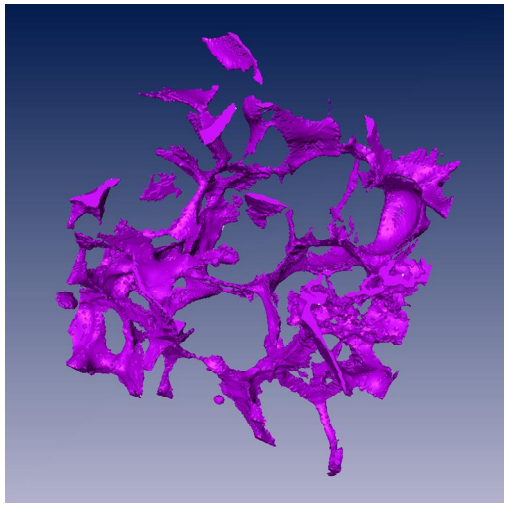

560°C (95%)

Morphology of the liquid phase

In situ 3D investigation of solidification (Al -4%Cu) using X-ray microtomography

ESRF-Grenoble

In O. Ludwig et al., Met. and Mat. Trans. 36A, June 2005, p. 1515.

Mesoscale granular model for globular microstructure

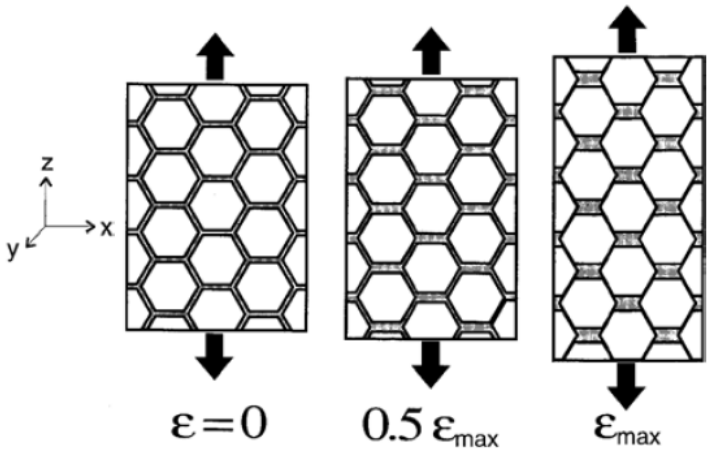

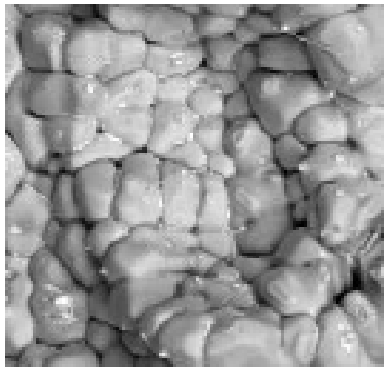

Globular microstructure
for grain refined alloys

- based on regular arrangement of grains
- all solid grains percolate at the same time when g_s =1

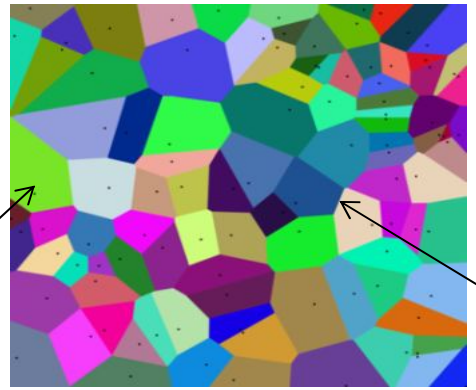

Nuclei

Voronoi tesselation

- based on the Voronoi diagram
- random set of nuclei

S. Vernède, PhD Thesis, Laboratoire de simulation des matériaux, EPFL, Lausanne, 2007.

Mesoscale granular model

Main advantages:

- **Provides a stochastic variation in grain size and shape**
- **Allows to account for the localization of straining, feeding and intergranular fracture**
- **Rather low computation cost**
- **Allows one to simulate a large number of grains, with a possible link with the macro scale**

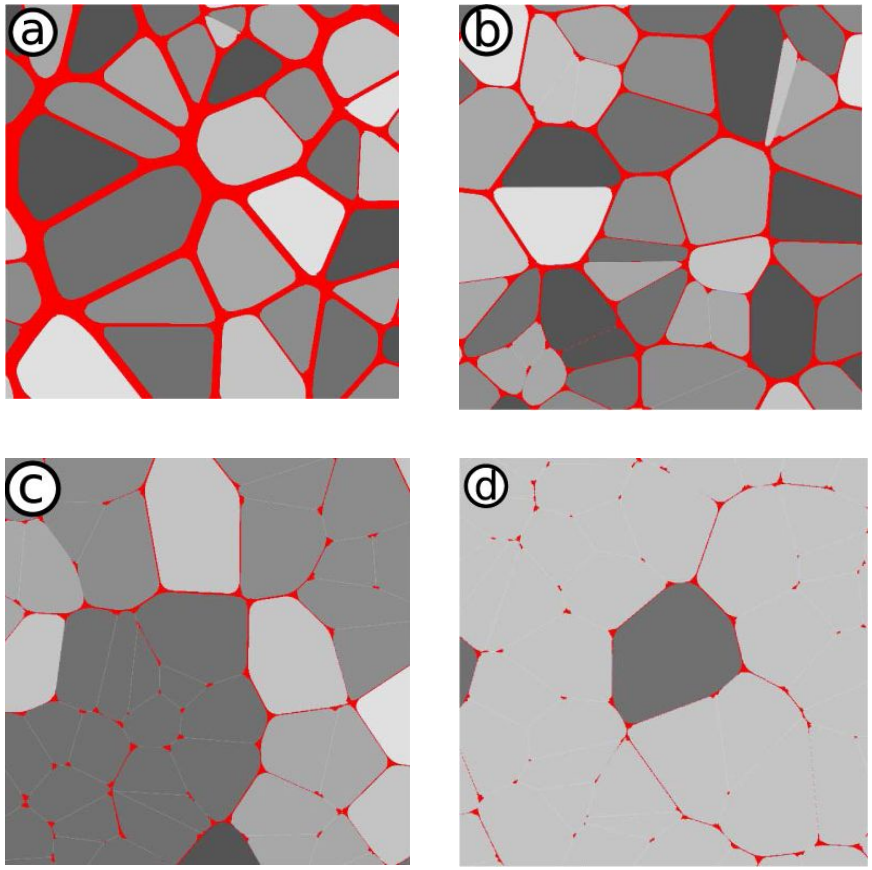

2D granular model (liquid is in red)

Granular model based on the Kirchhoff-Poiseuille with losses equations

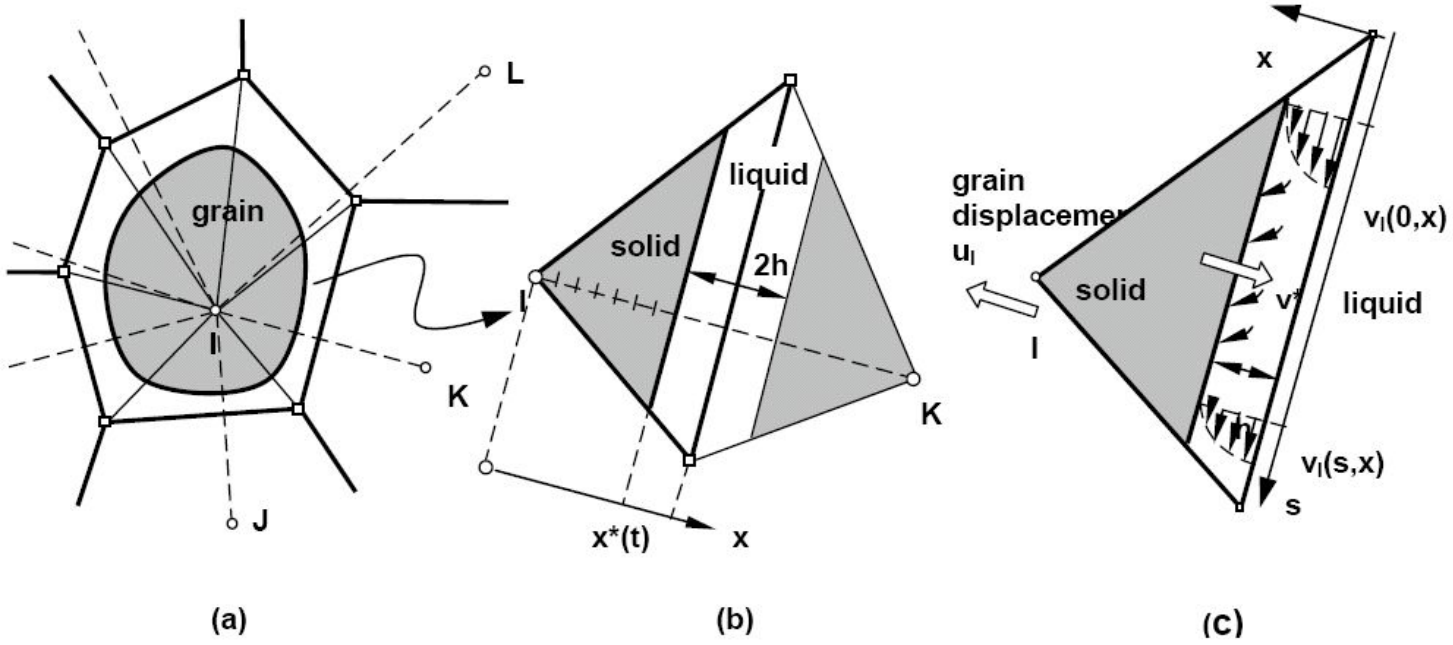

Granular model used for the simulation of solidification and feeding in a network of equiaxed globular grains: Voronoï tessellation (a), microsegregation model (b), feeding KPL model (c).

Pressure drop and fluid flow induced by solidification shrinkage

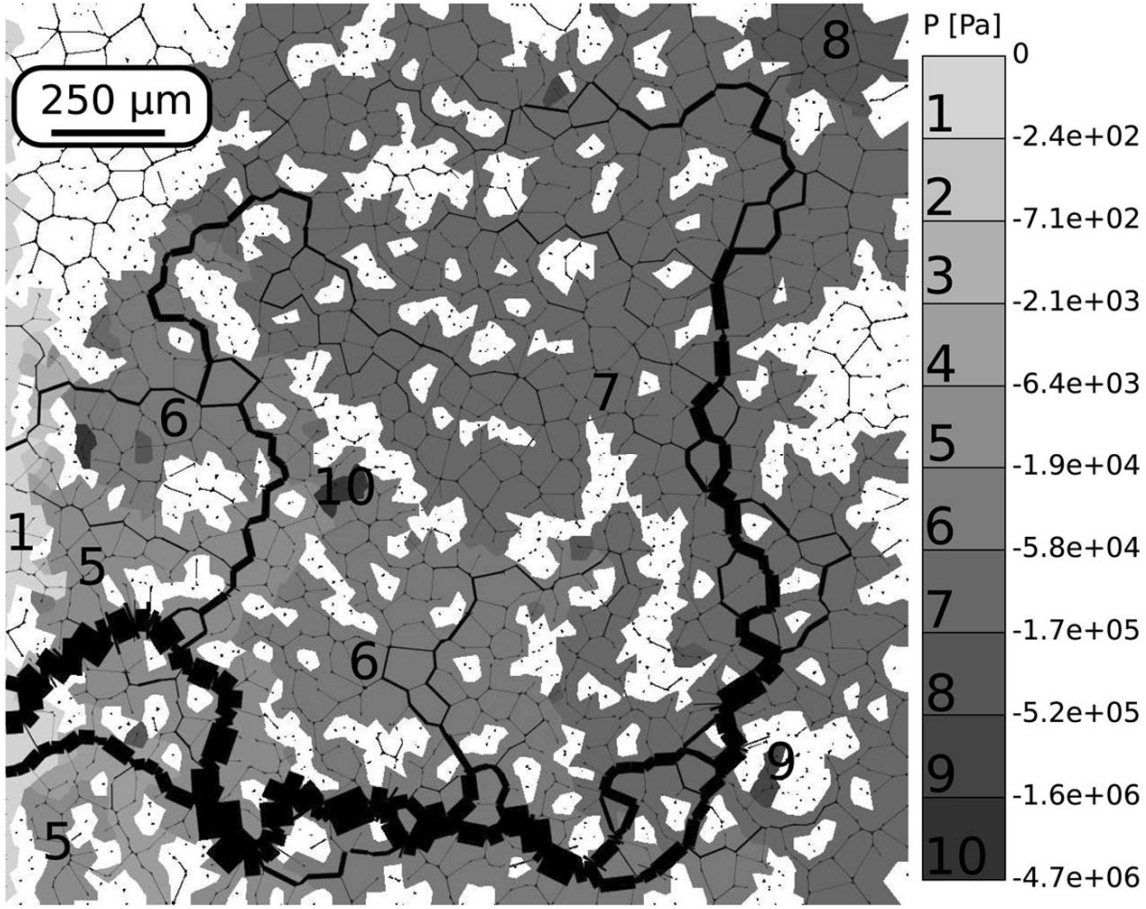

Al-1%Cu 2x2 mm2, 590°C, 98.4 % solid

The width of each channel is magnified proportionally to the local flow.

Gradual transition from a continuous intergranular film network to a continuous fully coherent solid

But no concomitance of percolation as observed in 3D

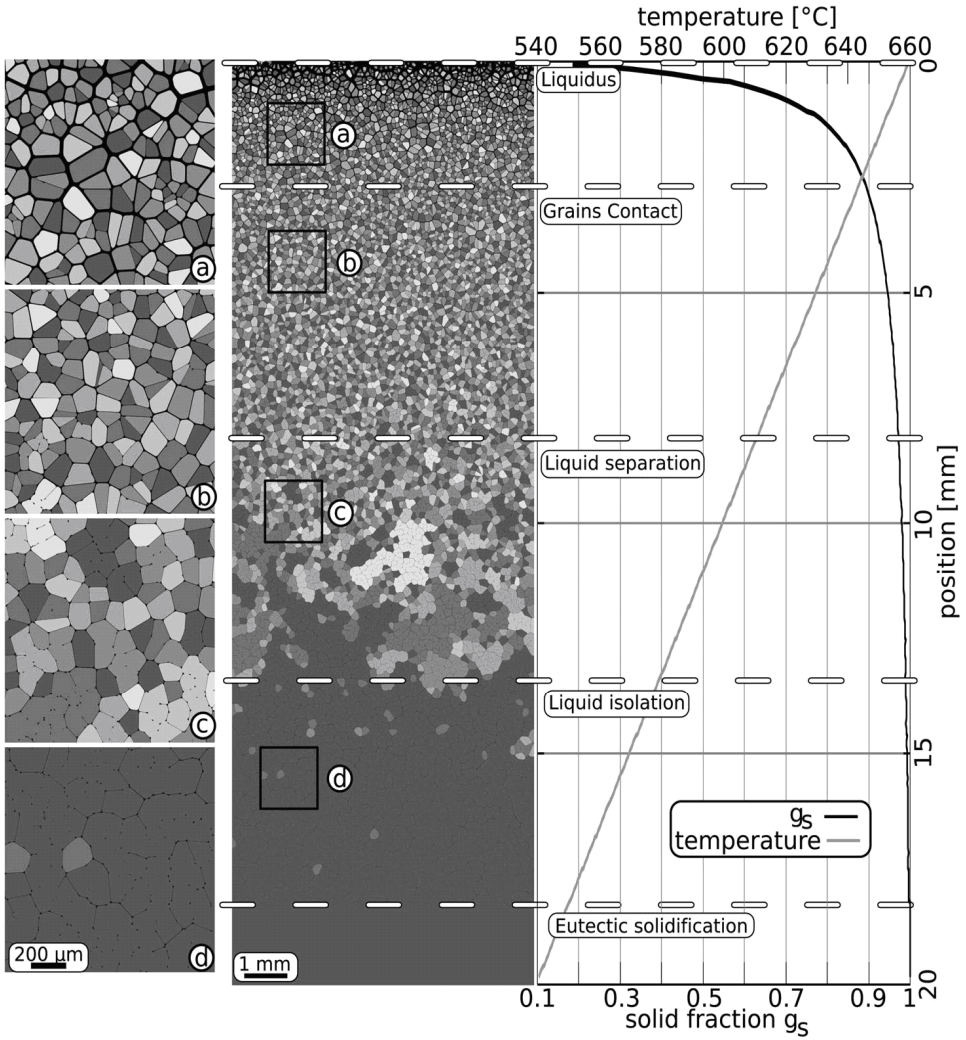

In region (a) (0 < gs < 0.89), most the grains are isolated and surrounded by liquid films.

In region (b) (0.89 < gs < 0.97), clusters of a few grains are formed but the liquid films remain continuous and interconnected.

In region (c) (0.97 < gs < 0.99), larger clusters are visible, with a few isolated liquid films remaining inside.

In region (d) (0.99 < gs < 1), the solid network is continuous and liquid only remains as isolated regions.

Gradual transition from a continuous intergranular film network to a continuous fully coherent solid

But no concomitance of percolation as observed in 3D

Tensile deformation at a given g_s

Semi-solid permeability, percolation, clustering, solid-liquid interfacial area, etc.

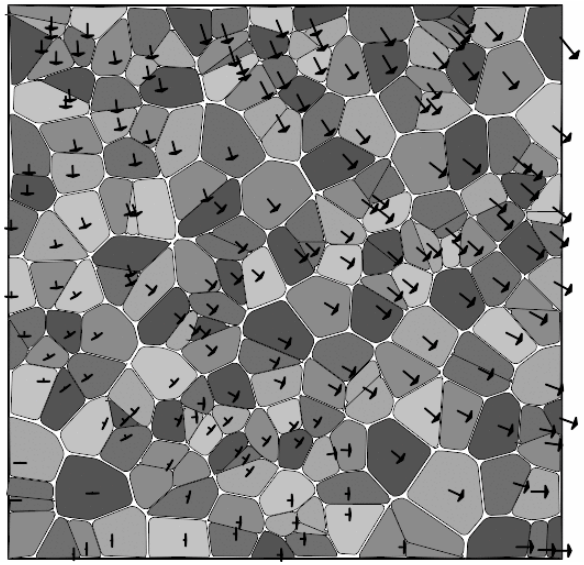

Displacement of the grains

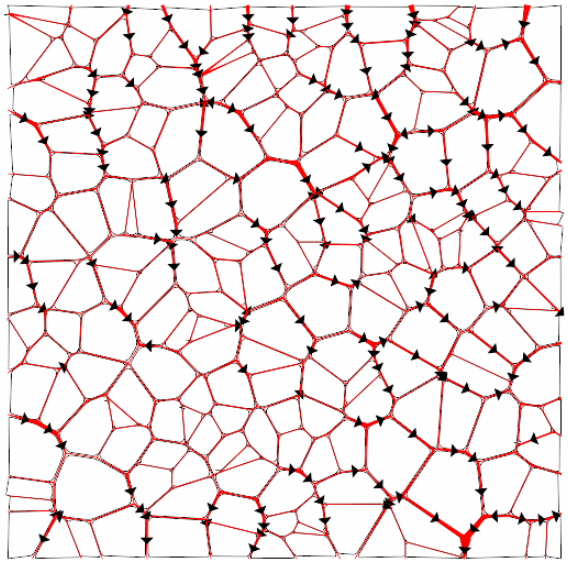

Flow of liquid

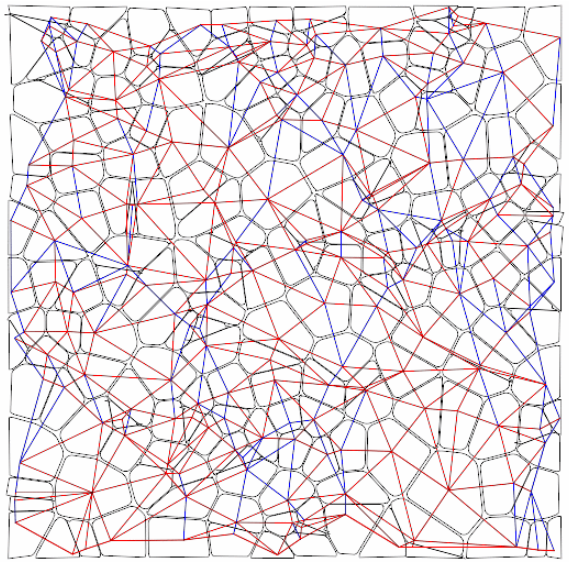

Stress build-up

S. Vernède, PhD Thesis, Laboratoire de simulation des matériaux, EPFL, Lausanne, 2007.

3D Mesoscale granular model for globular microstructure

- Grain geometry is derived from a Voronoi tessellation
- Each Voronoi region is divided up into small segments to model solidification
- Solidification is calculated based on a micro-segregation model with infinite mixing in the liquid and back-diffusion in the solid.

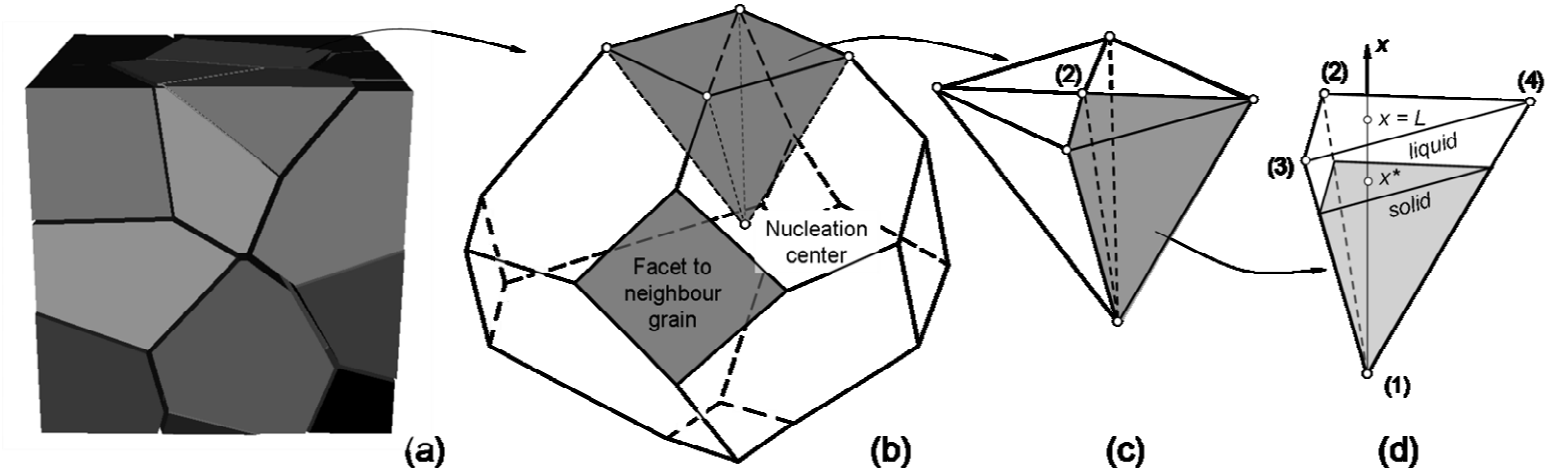

"dry" 3D granular model for globular microstructure

- Four types of elements are involved in the deformation model
  - Solid element
  - connector element
  - Multi point constraint element
  - Contact element

$$\sigma(\varepsilon, \dot{\varepsilon}, T) = k(T).\varepsilon^{n(T)}.\dot{\varepsilon}^{m(T)}$$

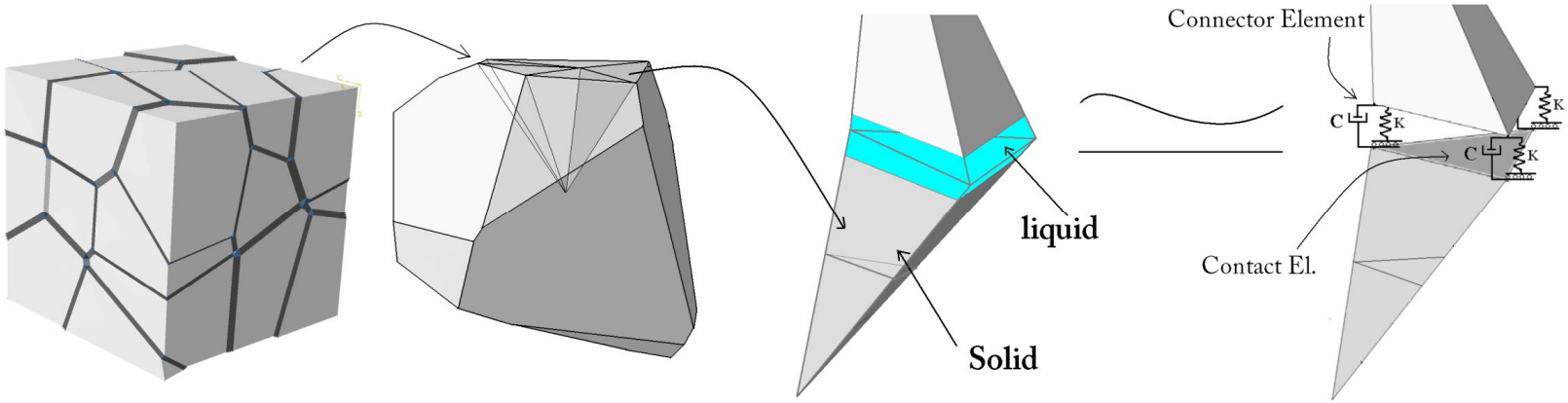

M. Sistaninia, A. Phillion, J. M. Drezet and M. Rappaz, submitted to *Met. and Mat. Trans.*

3D Mesoscale granular model for globular microstructure

- Solidification of Al-1wt%Cu
- 125 grains; CPU Time: 30s

- 98% solid
- Traction along x

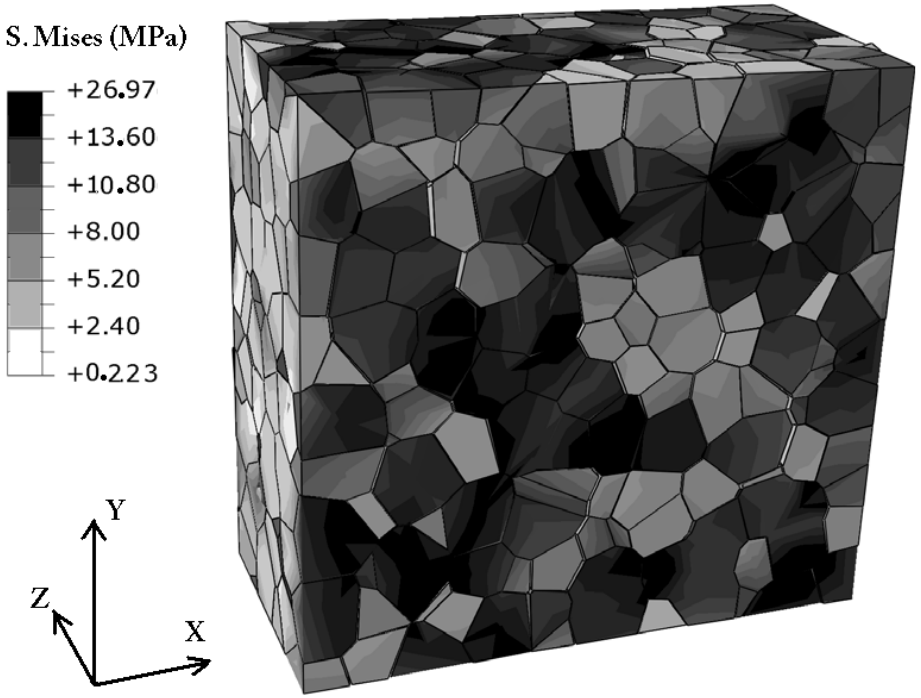

M. Sistaninia, A. Phillion, J. M. Drezet and M. Rappaz, submitted to *Met. and Mat. Trans.*

Tensile tests at different solid fractions

- **Tensile behaviour of partially solidified Al-Cu alloys**
- **Scaling (C, E) and validation of the semi-solid deformation model for different solid fraction**

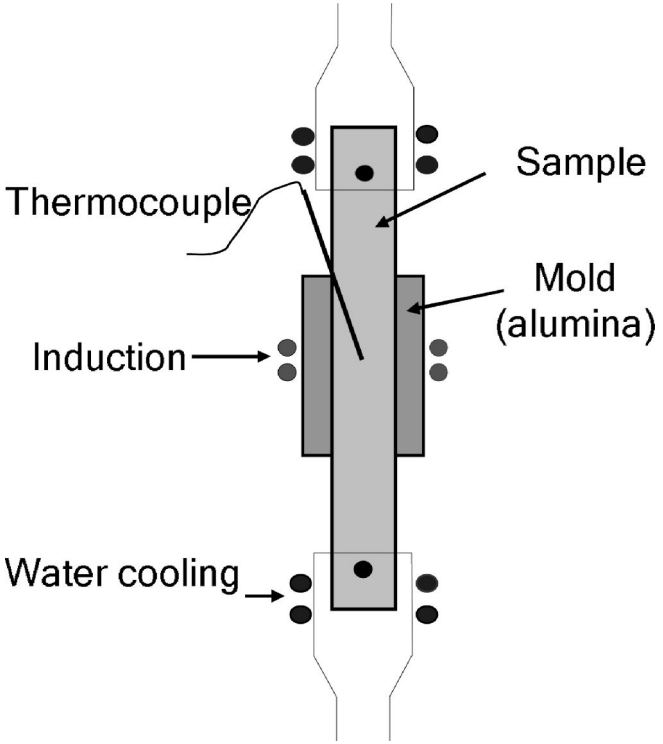

tensile experimental setup.

O. Ludwig, J. M. Drezet, C. l. Martin and M. Suéry, *Met. and Mat. Trans., vol.* 36A ,pp 1525-1535, 2005

"dry" 3D granular model for globular microstructure

Tensile tests at different solid fractions

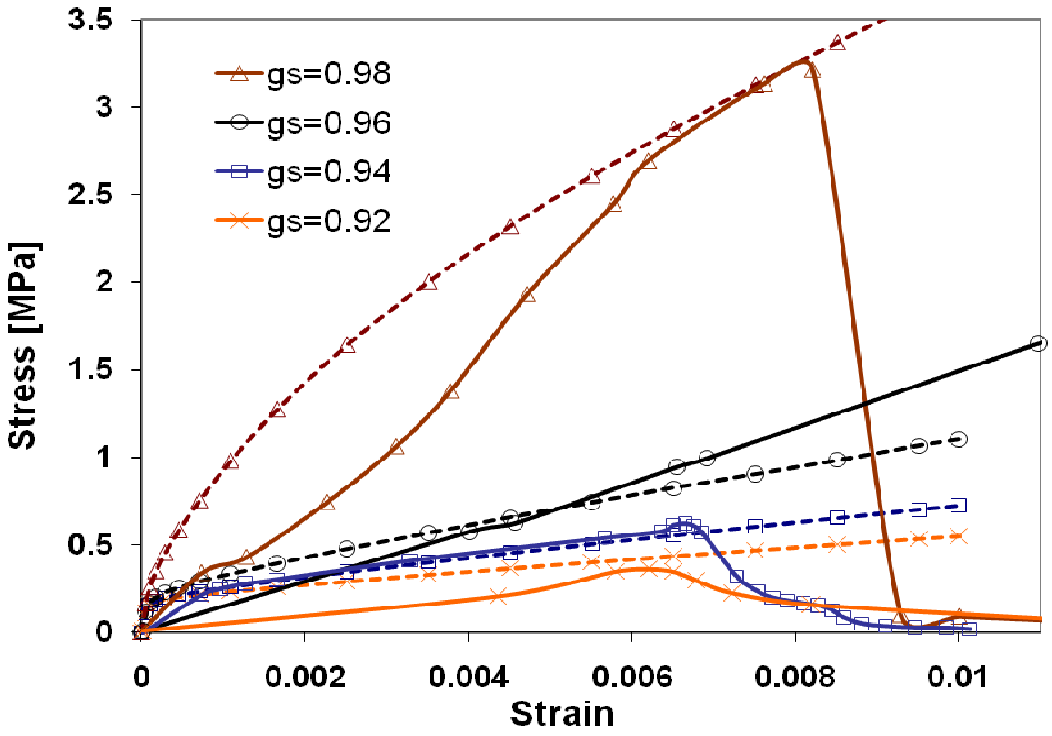

C = 2e3 N.S/m
K = 2.3 Mpa
determined at
gs = 94%
ε = 1e-3 /s

Experimental
Simulation

O. Ludwig, J. M. Drezet, C. l. Martin and M. Suéry, *Met. and Mat. Trans., vol.* 36A ,pp 1525-1535, 2005

M. Sistaninia, A. Phillion, J. M. Drezet and M. Rappaz, submitted to *Met. and Mat. Trans.*

Next step: inclusion of fluid flow within the 3D granular model

An extension of the 2D fluid flow model

Pressure drop calculation is performed assuming a Poiseuille flow

Flow losses compensating solidification shrinkage and semi-solid deformation

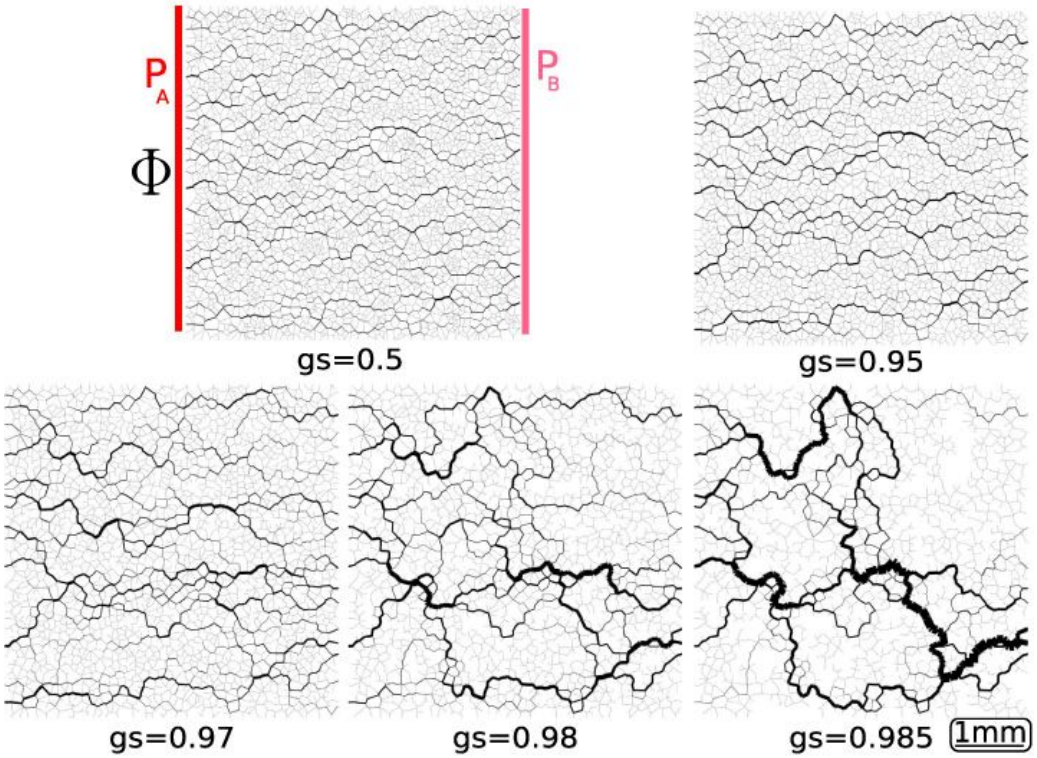

S. Vernède, P. Jarry, and M. Rappaz, *Acta Materialia, vol. 54, no. 15, pp. 4023-4034, 2006.*

Conclusion and perspectives

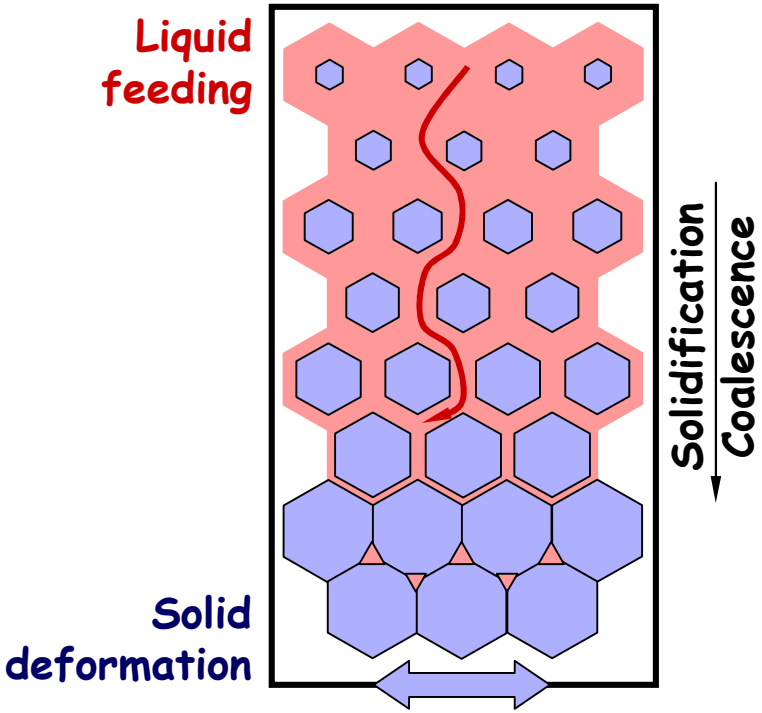

The coming challenge is to combine the three main phenomena :

- coalescence
- mechanical deformation
- and liquid feeding

using a 3D description

Model the hot tear formation as filmed by Terzi et al. at ESRF in Grenoble (X-ray microtomography)

- specimen of Al–8 wt.% Cu alloy
- cylinder of 2 mm in diameter and 8 mm in length
- heated up to 555 °C ($g_s \approx 0.91$)
- an average strain rate equal to 2×10^{-4} s^{-1}

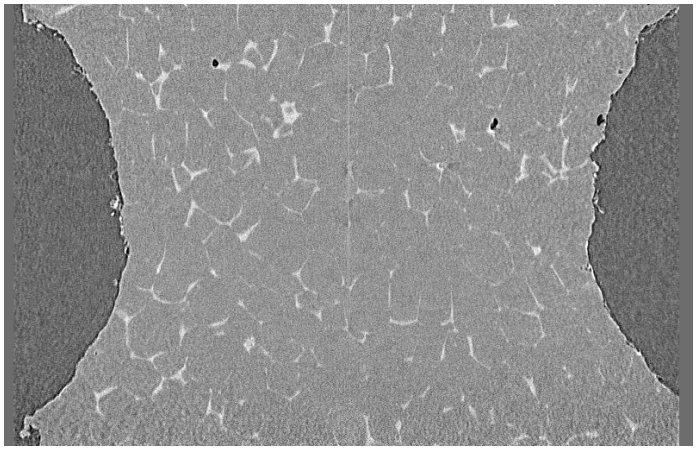

Terzi S, Salvo L, Suery M et al., Scripta Materialia, vol. 61, pp. 449-452, 2009

Strain concentrations :

$$\varepsilon^{th} = \beta \, \Delta T \, \frac{L}{l}$$

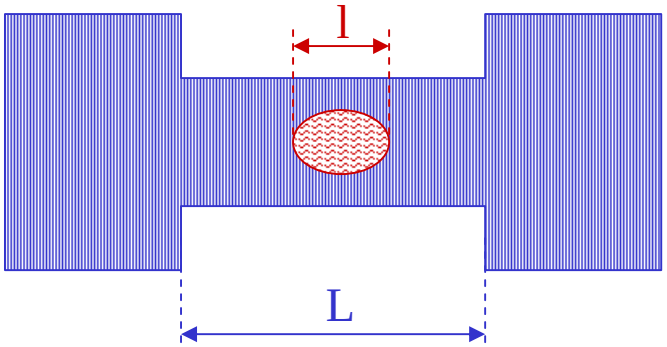

L : specimen dimension over which thermal contraction occurs
l : hot spot extension

Grain boundary concentrations :

$$\varepsilon^{th} = \beta \, \Delta T \, \frac{L}{l} \, \frac{\phi}{l}$$

J. Campbell

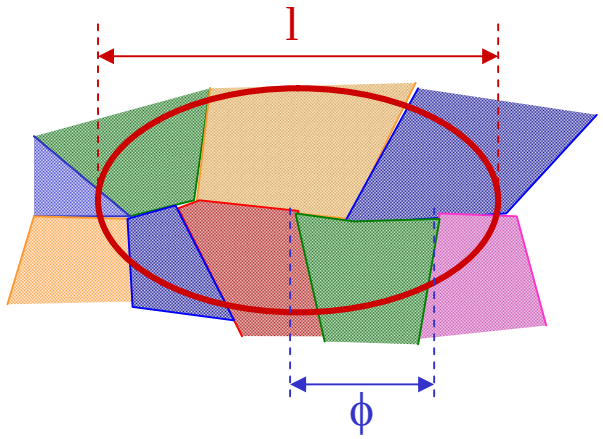

Essais de soudabilité : acier 9%Cr

Essais varestraint (installation CEA depuis 1990) : évaluation de la sensibilité à la fissuration à chaud de métaux d'apport

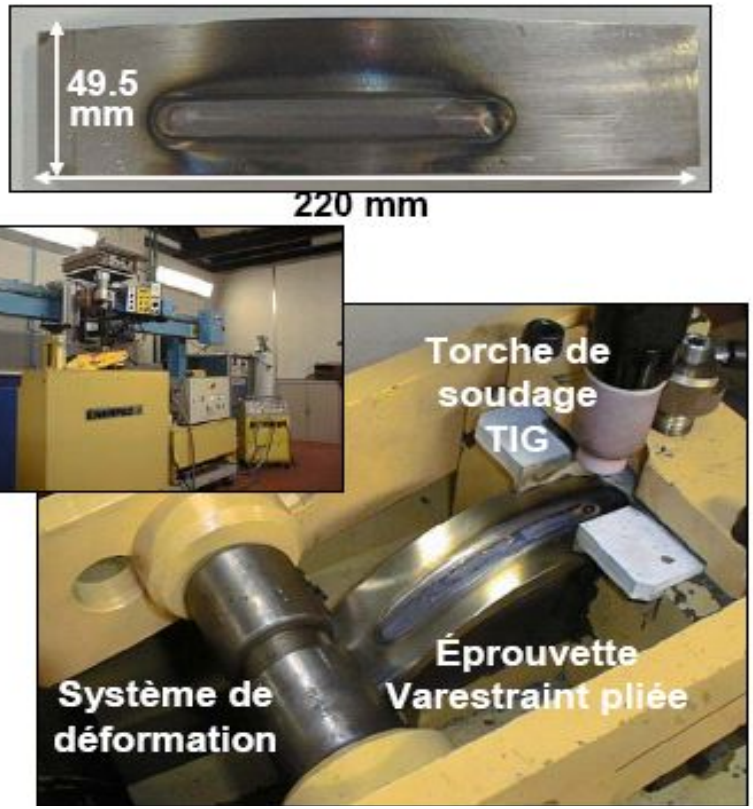

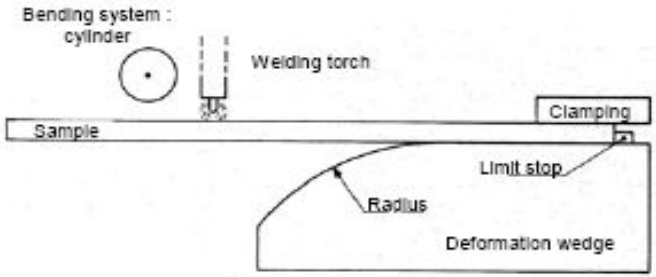

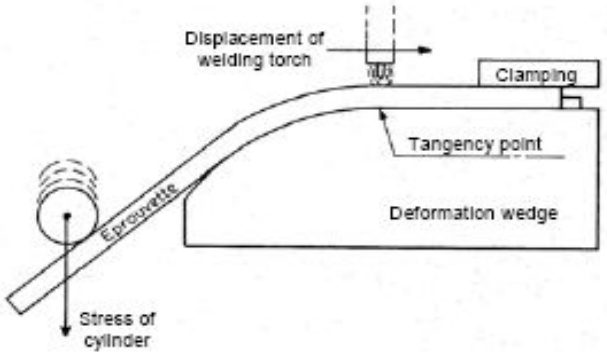

AISI SS 321 type